

RESEARCH LETTER

10.1002/2016GL070532

Key Points:

- Cooling contraction in volcanic rocks produces more numerous and larger cracks than heating expansion
- Thermal cracking produces largely isotropic crack orientations
- Both the rate and the energy of acoustic emissions are much higher during cooling than during heating

Supporting Information:

- Supporting Information S1

Correspondence to:

J. Browning,
j.browning@ucl.ac.uk

Citation:

Browning, J., P. Meredith, and A. Gudmundsson (2016), Cooling-dominated cracking in thermally stressed volcanic rocks, *Geophys. Res. Lett.*, 43, 8417–8425, doi:10.1002/2016GL070532.

Received 20 JUN 2016

Accepted 25 JUL 2016

Accepted article online 29 JUL 2016

Published online 18 AUG 2016

©2016. The Authors.

This is an open access article under the terms of the Creative Commons Attribution License, which permits use, distribution and reproduction in any medium, provided the original work is properly cited.

Cooling-dominated cracking in thermally stressed volcanic rocks

John Browning^{1,2}, Philip Meredith¹, and Agust Gudmundsson²

¹Department of Earth Sciences, University College London, London, UK, ²Department of Earth Sciences, Royal Holloway, University of London, Egham, UK

Abstract Most studies of thermally induced cracking in rocks have focused on the generation of cracks formed during heating and thermal expansion. Both the nature and the mechanism of crack formation during cooling are hypothesized to be different from those formed during heating. We present in situ acoustic emission data recorded as a proxy for crack damage evolution in a series of heating and cooling experiments on samples of basalt and dacite. Results show that both the rate and the energy of acoustic emission are consistently much higher during cooling than during heating. Seismic velocity comparisons and crack morphology analysis of our heated and cooled samples support the contemporaneous acoustic emission data and also indicate that thermal cracking is largely isotropic. These new data are important for assessing the contribution of cooling-induced damage within volcanic structures and layers such as dikes, sills, and lava flows.

1. Introduction

We present a generic study on the fracture development during heating and cooling of volcanic rocks, which is important as most studies to date have focused only on the heating part of a heating and cooling cycle [e.g., *Fredrich and Wong*, 1986; *Richter and Simmons*, 1974; *Simmons and Cooper*, 1978; *Meredith et al.*, 2001; *Vinciguerra et al.*, 2005]. A notable exception is the work of *Bruner* [1979, 1984] who modeled fracturing induced during the cooling and stress relaxation associated with unroofing of granite intrusions. Crustal segments hosting active (and therefore hot) magma chambers and associated intrusions experience complex stress regimes, commonly generated by a combination of regional tectonic forces and local the fluid pressures of magma chambers and intrusions (dikes, inclined sheets, and sills) [*Gudmundsson*, 2012]. While changes in stress around magma chambers have been widely studied [e.g., *Gudmundsson*, 2006], thermal stresses have received much less attention. Any thermal stressing produces damage in rocks [*David et al.*, 1999]. While we do not attempt to specifically model volcanic systems, the thermal stresses generated in such systems, like mechanical stresses, are likely to be generated cyclically [*Heap et al.*, 2013b] through new, hot magma received from time to time by the chamber and repeated intrusion and extrusion of magma. Such cyclicity may gradually produce additive rock damage, pushing the magma chamber toward failure, that is, rupture [*Browning et al.*, 2015]. In addition, the joints and fractures formed during this process also contribute to the formation of magma paths [*Gudmundsson*, 2011]. However, it is also possible that annealing and healing of fractures may occur at high temperatures between the main thermal-stress events. Some non-double couple earthquakes have been interpreted as being due to cooling and extension-fracture development (or formation) (columnar joints) related to the contraction of intrusions (e.g., thick sills) as well as large magma chambers [*Miller et al.*, 1998]. Non-double couple earthquakes have also been related to cooling and contraction of rocks due to fluid injection at geothermal sites [*Julian et al.*, 2010]. Targeted injection of cool fluids is a technique employed by the geothermal industry to force rapid contraction of the host rock around a borehole and force preexisting cracks to dilate and reopen or to form new extension fractures [*Brudy and Zoback*, 1999; *Kitao et al.*, 1990]. The aim is to increase reservoir permeability and fracture surface area and thereby enhance the efficiency of the geothermal system. In addition to these processes, it is likely that cooling-related fractures increase the permeability and rate of degassing of magma in shallow conduits [*Tuffen and Dingwell*, 2005; *Tuffen et al.*, 2003] as well as at the surface in viscous domes and lava flows [*Cabrera et al.*, 2011; *Gaunt et al.*, 2016].

When subjected to a change in temperature a rock mass will fracture when the thermal stresses generated by expansion or contraction of individual grains in contact with other grains reach the tensile or shear strength of the material. In the absence of thermal shock or high thermal gradients, thermal stresses are generated by two main mechanisms: (1) mismatch in thermal expansion coefficients between different minerals and

(2) thermal expansion anisotropy within single minerals. Hence, even in a monomineralic rock where the individual grains are randomly oriented stress will build up between grains on heating or cooling as they expand or contract by different amounts and in different directions. In a polymineralic rock the situation is exacerbated. In all the experiments reported here, samples were heated and cooled at low controlled rates so as not to induce thermal shock or high thermal gradients.

Here we report results from a series of experiments using a new apparatus designed to allow acoustic emissions (AEs) to be monitored during cracking associated with expansion and contraction of thermally treated cores of volcanic material. These experiments are used to test ideas on the magnitude and frequency of cracking due to thermal stresses, with a direct comparison between expansive and contractive stresses. Acoustic emissions, ultrasonic wave velocities, and microcrack analyses are used as proxies for understanding likely fracture modes. One difficulty when studying cooling-induced cracking in the laboratory is that the rock samples must necessarily be heated first so that post mortem studies will show a pattern of cracks generated partly during the heating and partly during the cooling part of the cycle. We therefore provide contemporaneous measurements of AE which act as a proxy for the number and relative size of microcracks. This data set is complemented by static measurements of ultrasonic wave velocities and microcrack image analysis of rocks both preheat and postheat treatments. The results presented form a generic study of thermal crack damage and are important over a range of volcanic environments and magmatic processes. Here, however, we focus primarily on the general process and mechanics of the thermal stressing.

1.1. Sample Characterization and Preparation

Two fine-grained igneous rock specimens were selected for the thermal stressing tests. An intrusive basalt from SW Iceland, Seljadalur basalt (SB), which has been widely used in rock physics studies [e.g., *Vinciguerra et al.*, 2005] and whose chemical and mechanical properties are well known. SB is a sill of tholeiite basalt dominated by an intergranular matrix of plagioclase, granular pyroxene, and iron oxides. Partially oriented plagioclase is found along with a rare abundance of augite, olivine, and an interstitial glass phase. SB has a density of $2900 \text{ kg/m}^3 \pm 10 \text{ kg/m}^3$, a mean grain size of $\sim 80 \mu\text{m}$, and an initial porosity of $\sim 4\%$. The second specimen is a high-silica extrusive dacite lava from the 1939–1940 Reck flow on Nea Kameni (NKD), Santorini [*Pyle and Elliott*, 2006]. The dacite lavas of Nea Kameni are petrophysically well studied [e.g., *Barton and Huijsmans*, 1986]; however, remarkably little work has been conducted on the mechanical properties of Santorini's recent lavas. NKD is a glass-bearing dacite with a density of $2200 \text{ kg/m}^3 \pm 10 \text{ kg/m}^3$, a fine-grained groundmass hosting $\sim 500 \mu\text{m}$ phenocrysts of plagioclase and an initial porosity of $\sim 10\%$. NKD has a porphyritic texture dominated by plagioclase, pyroxene, iron oxides, and rare sanidine. Since the dacite lava is extrusive it has undergone a cooling history very different from that of the basaltic sill. Core samples with a diameter of 25 mm and a length of 70 mm were prepared from both rock types with their end surfaces ground flat and parallel using a surface grinder.

1.2. Experimental Apparatus and Calibration

Core samples were held within a purpose-built testing jig manufactured from 310 steel alloy capable of sustaining temperatures up to 1100°C without significant corrosion. The jig is $\sim 1 \text{ m}$ in length and comprises a series of rods and springs to hold the sample under constant end-load within the central, uniform temperature section of a Carbolite CTF12/75/700 tube furnace while allowing for expansion and contraction, as illustrated in Figure 1. The central rods act as acoustic waveguides and are of sufficient length to enable the AE transducer to be located outside the furnace where it remains cool. The external springs allow the central rods to move in response to sample expansion and contraction during heating and cooling while also allowing a uniform contact between the waveguide and sample to be maintained throughout the experiments. Temperature was controlled by a multistage programmable temperature controller via a signal fed from a thermocouple within the furnace. Sample temperature was measured by a second thermocouple attached directly to the sample surface. All experiments were conducted at ambient pressure.

Prior to conducting any thermal cracking experiments on the samples, we ran a series of calibration experiments to quantify the thermal gradient within the samples and the level of acoustic noise generated by the testing jig. Using two thermocouples, we were able to establish that the temperature difference across our samples was $\sim 1^\circ\text{C}$ at a heating rate of $1^\circ\text{C}/\text{min}$, and using a noncracking glass sample, we found that the AE "noise" was less than 1% of that generated using our rock samples (see supporting information for further details).

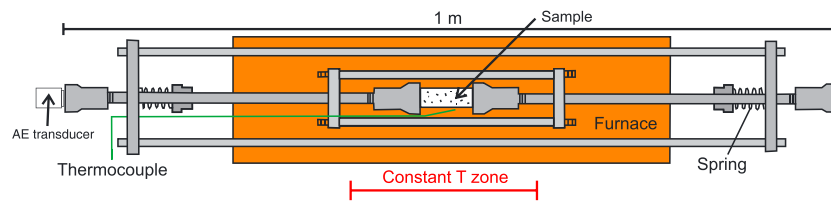


Figure 1. Experimental arrangement used for thermal stressing experiments. The 1 m stainless steel jig assembly clamps the sample centrally within the constant temperature zone of the furnace while allowing for expansion and contraction. The central rod acts as an acoustic wave guide with an AE recording transducer clamped to one end.

2. Methodology

In all thermal stressing tests, samples were heated at constant rates of either 1 or 8°C/min in order to investigate the effects of different heating rates. After heating to a predetermined maximum temperature, the samples were then held at that temperature for 30 min, more than sufficient to allow for temperature equilibration (supporting information). Samples were then cooled at one of two rates, either a constant controlled rate of 1°C/min or the natural cooling rate (which varies as a function of temperature above ambient). In order to capture dynamic crack growth and nucleation events during our thermal stressing tests we record contemporaneous acoustic emissions (AEs). A Panametrics V103 piezoelectric P wave transducer was attached to the end of one of the steel wave guides. The received signal was then passed through a preamplifier and recorded using a Vallen AMSY-5 acoustic emission analyzer connected to a PC. For each AE hit, we record both the arrival time and the full waveform. The arrival times are used to calculate the hit rate, which can be used as a proxy for the contemporary rate of cracking. The area under the envelope of each discrete waveform provides a measure of the energy of each AE hit, which acts as a proxy for the relative size of the associated increment of crack extension (see *Cox and Meredith [1993]* for a detailed description of the AE recording method and analysis).

3. Results

3.1. AE and Thermal Cracking

In Figure 2 we plot AE energy and temperature as a function of time for both SB and NKD and at two heating rates, 1°C/min and 8°C/min, respectively. In every test, both the AE hit rate and the energy were notably higher during the cooling part of the thermal treatment cycle than during the heating part of the cycle (Figure 2 and Table 1). The onset of sustained output of AE occurs at a very similar temperature of around 800°C during cooling in all experiments. Although SB produces a significantly higher rate of AE energy output at higher heating and cooling rates, this effect is less apparent for NKD. The lowest AE rates occur consistently during the hold periods at maximum temperature, which suggests that thermal equilibration is reached and that any thermal stress is therefore minimized.

In Table 1 we provide a quantitative comparison of the AE statistics. Specifically, we compare the number of AE hits and the hit rate, together with the AE energy and energy rate, for both rock types during a 1°C/min heating and cooling cycle. This is a useful comparison, because both the heating and the cooling parts of the cycle have the same duration in these tests. By contrast, a direct comparison of AE data for tests at higher heating rates and the natural cooling rate is not meaningful because the duration of the cooling phase is much greater than the heating phase. In each case in Table 1, it is clear that, significantly, more AE is generated during cooling than during heating.

3.2. Acoustic Wave Velocities and Crack Distribution

Radial P wave velocity (V_p) as a function of azimuth is reported in Figure 3 alongside crack distribution maps. The P wave velocity for as-received Seljadalur basalt (SB) is 5.52 ± 0.12 km/s and for Nea Kameni Dacite (NKD) is 5.29 ± 0.04 km/s. The variation with azimuth is very small, and both materials are essentially isotropic. Following heat treatment of SB to 1100°C and NKD to 800°C, the P wave velocities decreased substantially for all samples along all azimuths so that the isotropy was maintained. Velocity decreases are most significant in SB where V_p dropped by around 45% to a mean value of 3.03 ± 0.17 km/s. For NKD, the decrease was smaller but still significant; by around 21% to a mean value of 4.15 ± 0.10 km/s.

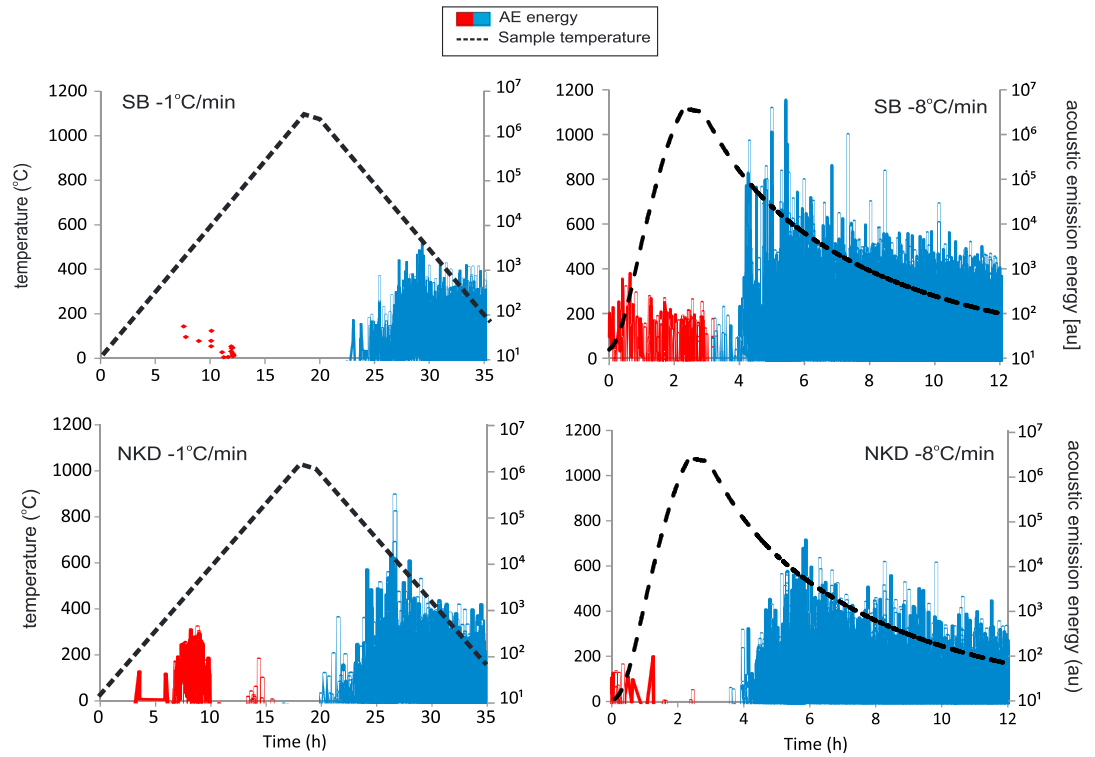


Figure 2. Acoustic emission energy and temperature over time for two rock types (Seljadalur Basalt, SB, and Nea Kameni Dacite, NKD) and two different heating (1°C/min and 8°C/min) and cooling rates (black dashed lines). Red indicates AE generated during the heating phase, and blue indicates AE generated during the cooling phase.

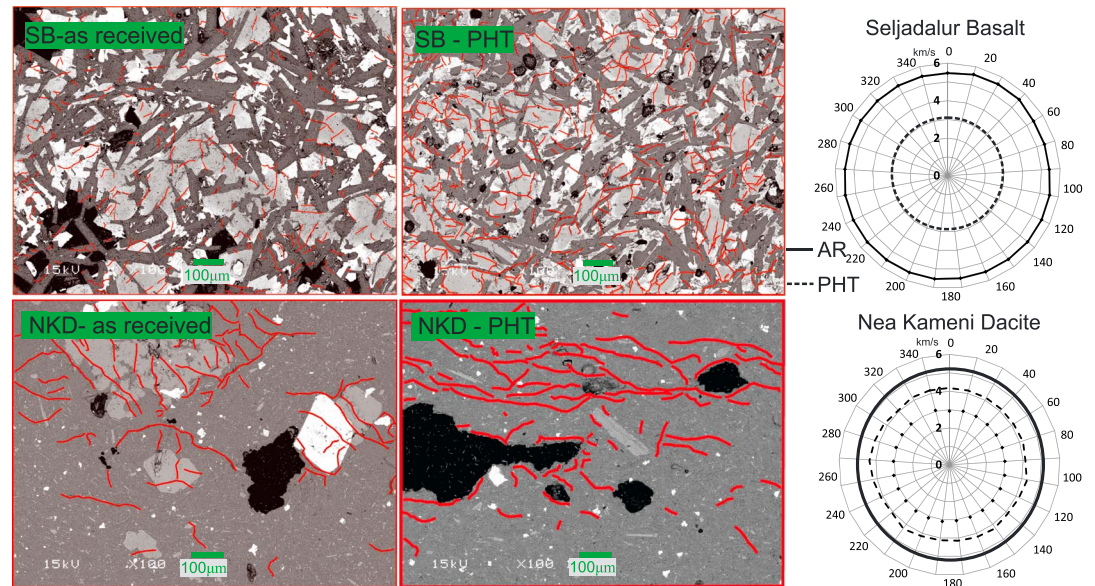


Figure 3. SEM image and measured crack distribution map from an as-received, nonheat treated SB basalt sample, and NKD dacite. SEM image and measured crack distribution map from an experimentally heat-treated basalt sample to 1100°C (SB-PHT) and dacite to 800°C (NKD-PHT). Radial *P* wave velocities for SB and NKD are indicated for as received (solid line) and postheat treatment (dashed line) samples.

Table 1. Acoustic Emission Hits, Hit Rates, Energy, Energy Rates, and Energy/Hit (\bar{E}) for a 1°C/min Heating and Cooling Test on Seljadalur Basalt (SB) and Nea Kameni Dacite (NKD)^a

Heating/Cooling Rate = 1°C/min	Total Hits	Hit Rate (min ⁻¹)	Total Energy (AU)	Energy rate (min ⁻¹)	\bar{E} (AU)
<i>SB heating</i>	42	0.04	8.0×10^2	0.4	19
SB cooling	6166	6.45	3.8×10^5	3.9×10^2	62
<i>NKD heating</i>	1310	1.60	2.5×10^4	30	19
NKD cooling	8573	9.02	1.0×10^6	1.0×10^3	117

^aItalicized text indicates acoustic emissions recorded during heating. Bold text indicates acoustic emissions recorded during cooling.

Crack distributions were mapped and analyzed from SEM imagery, from the same core of both as-received and heat-treated samples. As-received SB samples exhibited an abundance of preexisting microcracks that were generally evenly distributed throughout the samples. The cracks ranged in length from approximately 25 μm to 150 μm . Heat treatment appeared to substantially increase the total number of cracks but did not significantly increase their average length. Cracks were essentially isotropically oriented and distributed homogeneously throughout. The total number of cracks in SB increased by around 42% following heat treatment, while for NKD the increase was lower at around 20%. Clearly, the SEM images provide only a two-dimensional view of a three-dimensional problem, so we consider the recorded increases to represent a minimum change. They also do not allow us to discriminate between cracks generated during heating and cooling. Furthermore, the as-received and heat-treated crack distributions were measured on different samples, so the data need to be interpreted with caution due to natural sample variability.

Nevertheless, both the ultrasonic wave velocity and the image analysis data act to support our contemporaneous AE data and show that significant cracking occurs as a result of thermal stressing.

4. Discussion

Most studies dealing with thermal cracking in rocks have concentrated on cracking during heating [e.g., Richter and Simmons, 1974; Simmons and Cooper, 1978; Fredrich and Wong, 1986; Meredith et al., 2001; Vinciguerra et al., 2005]. A few studies have presented anecdotal evidence of substantial cracking during cooling [e.g., Heap et al., 2013a; Mollo et al., 2013] and one [Bruner, 1979, 1984] modeled fracturing induced by the cooling and unroofing of granite intrusions.

As we noted earlier, a major problem when studying cooling-induced cracking in the laboratory is that the rock samples must necessarily first be heated. All post-test samples therefore necessarily exhibit cracking that was generated partly during the heating phase and partly during the cooling phase of the experiment. Hence, comparative pre-test and post-test measurements on thermally treated samples, such as ultrasonic wave velocities and image analysis, are inherently unable to discriminate between heating-induced cracks and cooling-induced cracks. We therefore use the AE output, which is measured contemporaneously with temperature during both heating and cooling, as our primary data source for monitoring the evolution of thermal cracking.

In order to highlight the differences between heating-induced and cooling-induced microcracking, we provide a comparison between the number and average energy of AE hits generated during both the heating and the cooling phases of tests conducted at heating and cooling rates of 1°C/min on samples of both SB and NKD in Table 1. We find that the vast majority of AE energy results from thermal cracking generated during the cooling phase rather than during the heating phase; 99.8% for SB and 97.5% for NKD. As for SB, not only are there 147 times as many hits during the cooling phase as during the heating phase, but their average energy is also more than 3 times greater, resulting in a total AE energy that is approximately 500 times higher. The implications are that many more cracks were generated during cooling and, also, that their average size is larger. A similar, although less spectacular, result is seen for NKD, where the number of hits during cooling is 6.5 times higher, while their average energy is 6 times greater; resulting in a total AE energy that is about 40 times higher. So, the key questions are the following: (1) why is there so much more cracking generated during cooling than during heating and (2) what are the mechanisms responsible?

4.1. Mechanical Processes Responsible for Thermal Cracking

In the absence of thermal shock, thermal cracking is generated by thermal expansion anisotropy within single-mineral phases and thermal expansion mismatch between different mineral phases. Meredith et al.

[2001] studied the microscopic origin of thermal cracking and quantified the thermal stresses produced by thermal expansion anisotropy using neutron diffraction to analyze the thermal strains generated within the crystallites of a pure quartzite during heating. They measured the thermal strains induced in the quartzite and compared them with the thermal strains induced in a quartz powder produced by comminution of the same rock. Each grain in the unconstrained quartz powder was free to expand fully, whereas each grain in the quartzite was partially constrained by the expansion of its neighboring grains. This internal self-constraint leads to a large thermal strain deficit in the quartzite in the high-expansion (a axis) direction and a small thermal strain excess in the low-expansion (c axis) direction. These strain differences are maintained by the generation of anisotropic thermal stresses. Thermal cracking, evidenced by a large burst of AE activity, commenced around 190°C when the induced thermal stress exceeded a value close to the tensile strength of the quartzite. The mechanism responsible for the thermal cracking is thus considered to be tensile fracturing due to high compressive stresses along the a axes of quartz grains, aided by small, orthogonal tensile stresses along their c axes.

Fredrich and Wong [1986] studied thermal cracking during heating of three crustal rocks, two of which are polymineralic (Westerly granite and Frederick diabase). They explained their data using a fracture mechanics model that took account of both thermal expansion anisotropy and thermal expansion mismatch. In the granite, grain boundary cracking occurred over a relatively narrow temperature range; commencing at 100° to 165°C, with a substantial proportion cracked by 250°C (and all cracked by 500°C). Most of these cracks terminated at geometrical discontinuities along the grain boundaries. Intragranular cracks were seen to grow at similar rates to the grain boundary cracks up to 250°C but then at a much higher rate above this temperature. These cracks initiated at grain boundaries and propagated approximately normal to them until terminating at some point within the grain interior (i.e., before becoming transgranular cracks). Thermal cracking in the diabase required significantly higher temperatures, with very little cracking below 500°C and significant crack densities only observed in samples heated above 1000°C. It was not possible to quantify the relative contributions of grain boundary versus intragranular cracking in this rock.

Inclusion models are commonly used for the analysis of thermal cracking. Most early studies [e.g., *Evans*, 1974; 1978; *Johnson et al.*, 1978; *Wang and Heard*, 1985] considered spherical inclusions for mathematical convenience. One problem is that while there are no sharp corners on a sphere, observations of *Fredrich and Wong* [1986] show that many thermal cracks nucleate from and terminate at geometrical discontinuities. Their model therefore considers the effect of a homogeneous temperature increase on the internal stress field of an angular inclusion embedded within an effective medium. Many complicated geometries could be analyzed, but *Fredrich and Wong* [1986] concluded that a relatively simple square inclusion captured all the key features. They obtained analytical solutions for the mode-I (tensile) stress intensity factor of microfractures in close proximity to the square inclusion as a function of normalized crack length (crack length divided by inclusion edge length) for both thermal expansion anisotropy and thermal expansion mismatch. For thermal expansion anisotropy, their analysis showed that crack growth was inherently stable with the stress intensity factor peaking at normalized crack lengths of about 0.2 for grain boundary cracks and about 0.3 for intragranular cracks. For thermal expansion mismatch, they found that intragranular cracking ceased at normalized crack lengths greater than about 0.3, but that grain boundary cracking was inherently unstable, with the stress intensity factor increasing for all crack lengths. Such cracks are therefore predicted to propagate along the whole grain boundary and only terminate at a geometrical discontinuity (the corner of the square inclusion in their model).

As noted earlier, *Bruner* [1979, 1984] modeled fracturing induced by the unroofing of granite intrusions. His analysis is expected to predict unstable cracking under all conditions (as noted by *Fredrich and Wong* [1986]). This may be because, in considering unroofing, his analysis inherently considers both cooling and depressurization. We therefore consider that the most appropriate scenario within which to interpret our data is that of *Fredrich and Wong* [1986] with the signs changed to take account of both heating and cooling.

Considered within this framework, our observations suggest that the low AE energy generated during heating, within an overall compressional regime, is likely associated with small increments of extension of preexisting grain boundary cracks and the growth of a relatively small number of new, intragranular microcracks. By contrast, the very high AE energy generated during cooling, within an overall tensile regime, is likely associated with the formation of a significant number of full-length, tensile grain boundary cracks plus significant increments of limited intragranular crack growth (especially at the highest temperatures). Our interpretation of the contemporaneous AE data is supported by the complementary measurements and observations on

preheat and postheat treated rocks that show substantially reduced seismic velocities and increased numbers and lengths of cracks in postheat-treated samples.

We therefore suggest that earlier studies which analyzed thermal cracking only occurring during the heating phase [e.g., Jones *et al.*, 1997] substantially overestimate the thermal crack damage induced by heating and substantially underestimate the amount of thermal damage induced during cooling. We propose that the amount of crack damage induced during cooling differs between our two rock types because of their different cooling histories following emplacement. Extrusive lavas such as NKD experience faster cooling and significant degassing which results in the development of vesicles and an extensive microcrack network. Thermal treatment has thus less noticeable effect than that experienced in rocks formed in an intrusive environment, such as SB. The difference between damage generated during the heating phase and the cooling phase can be explained in terms of the overall state of stress within the sample. It is well known that the tensile strength (T_o) of materials is substantially lower than the compressive strength (σ_c), where $T_o \approx 0.1\sigma_c$ [e.g., Gudmundsson, 2011]. It is therefore much easier for cracks to form in the overall tensile regime created during cooling and contraction as oppose to the overall compressive regime created during heating and expansion.

4.2. Scaling of Experimental Data to Natural Conditions

Laboratory AE signals obey a power law relationship with source dimension (increment of crack growth), just as field scale seismicity does; permitting similar statistics to be used to describe them both [Main, 1992; Hatton *et al.*, 1994]. Thus, although AE and seismic signals are very different in absolute values of frequency and magnitude, they can be linked through frequency-length scaling [Aki and Richards, 1980], which offers a robust method to assess the equivalence of physical processes between laboratory experiments and natural events. In particular, Burlini *et al.* [2007] demonstrated that AE waveforms generated by thermal cracking during laboratory experiments had remarkably similar spectrograms to those generated during low-frequency volcanic events [McNutt, 2000]. Further studies have also shown that these scaling relationships hold for a wide range of deformation processes, including volcanic long-period seismicity [Benson *et al.*, 2008] and seismic tremor [Burlini *et al.*, 2009] in spite of the very different temperature rates; suggesting that the same underlying physical processes are operative. For our experimental samples, the thermal cracking events during cooling have a dominant frequency of ~ 1 MHz for crack increments from ~ 82 to $500 \mu\text{m}$ (from microstructural measurements of cracks in SB and NKD, respectively). In nature, low-frequency volcanic events are reported to have dominant frequencies of 1–5 Hz associated with fracture lengths of hundreds to 1000 m [McNutt, 2000; Burlini *et al.*, 2007]. In consideration that dominant frequencies of seismic events (f) scale inversely with source dimension (d) [Aki and Richards, 1980], we may write $d_F/d_L = f_L/f_F$, where the subscripts L and F denote measurements at the laboratory and field scale, respectively. Comparing our laboratory data with the typical frequency and size of low-frequency volcanic events, we obtain $f_L/f_F = 2\text{--}10 \times 10^5$ and $d_F/d_L = 6\text{--}40 \times 10^5$, indicating agreement between the laboratory and field cases within a factor of 3 to 4 over 6 orders of magnitude. Of course, it would be better if we were able to compare our laboratory results directly with data from natural thermal cracking events, but no such comparable data are available in the literature. However, if we consider natural cases such as columnar jointing or cooling cracks in the surface layers of lava flows, dimensions in the range 0.2–20 m are commonly reported [e.g., Budkewitsch and Robin, 1994]. Hence, we might anticipate associated seismicity with frequencies from about 10 Hz to about 1 kHz. We therefore consider it a priority for further research on this subject to measure simultaneously the crack length and frequency of associated seismic signals generated during natural thermal cracking events on volcanoes.

5. Conclusions

Our measurements and observations show that heating and resultant thermal expansion in volcanic rocks acts to extend preexisting microcracks by only small increments or nucleate a relatively small number of new microcracks. By contrast, contraction during cooling from high temperature encourages the growth and extension of many more and larger, predominantly tensile, microcracks.

The results suggest that there is far more cracking during cooling than during heating. This is reflected in contemporaneous acoustic emission data that show substantially higher AE rates and energies during cooling than during heating. These high AE rates commence shortly after the onset of cooling and continue throughout the cooling phase. Evidence from ultrasonic wave velocities and microstructural analysis shows that thermal cracking is isotropically distributed. This is expected because thermal stresses are by nature

isotropic. Furthermore, cooling and contraction generates an overall tensile stress which encourages crack formation and growth because rocks are weaker in tension than compression.

These findings have important implications for the study of the cooling of volcanic rocks in a range of different settings. It is already well known that extrusive lava flows such as those on Mt. Etna contain substantially more crack damage than intrusive rocks, as noted from their lower *P* wave velocities [Vinciguerra *et al.*, 2005]. Our observations show clearly that very significant amounts of crack damage are likely to be generated during the emplacement and subsequent cooling of volcanic rocks, with implications for permeability and associated movements of crustal fluids.

Acknowledgments

We are grateful for continuous support from S. Boon and N. Hughes who were heavily involved with the experimental apparatus design. We thank K. Drymoni, Y. Lavallée, and F. Von Aulock for assistance with thermal characterization of our materials, T. Mitchell for assistance with micro-structural characterization, and H. Reynolds for discussion throughout. We also thank the Editor A. Newman as well as S. Vinciguerra and an anonymous reviewer for comments which greatly improved this manuscript. J.B. acknowledges an RHUL Reid Scholarship and a UoL Central Research Grant award. This study was partially funded by NERC project NE/N002938/1. Supporting data are included in the supporting information; any additional data may be obtained from J.B. (email: j.browning@ucl.ac.uk).

References

- Aki, K., and P. G. Richards (1980), *Quantitative Seismology: Theory and Methods*, 932 pp., W.H. Freeman, San Francisco, Calif.
- Barton, M., and J. P. Huijsmans (1986), Post-caldera dacites from the Santorini volcanic complex, Aegean Sea, Greece: An example of the eruption of lavas of near-constant composition over a 2200 year period, *Contrib. Mineral. Petrol.*, *94*, 472–495.
- Benson, P. M., S. Vinciguerra, P. G. Meredith, and R. P. Young (2008), Laboratory simulation of volcano seismicity, *Science*, *322*, 249–252, doi:10.1126/science.1161927.
- Browning, J., K. Drymoni, and A. Gudmundsson (2015), Forecasting magma-chamber rupture at Santorini volcano, Greece, *Sci. Rep.*, *5*, doi:10.1038/srep15785.
- Brudy, M., and M. Zoback (1999), Drilling-induced tensile wall-fractures: Implications for determination of in-situ stress orientation and magnitude, *Int. J. Rock Mech. Min. Sci.*, *36*, 191–215.
- Bruner, W. M. (1979), Crack growth and the thermoelastic behaviour of rocks, *J. Geophys. Res.*, *84*, 5578–5590, doi:10.1029/JB084iB10p05578.
- Bruner, W. M. (1984), Crack growth during unroofing of crustal rocks: Effects of thermoelastic behaviour and near-surface stresses, *J. Geophys. Res.*, *89*, 4167–4184, doi:10.1029/JB089iB06p04167.
- Budkewitsch, P., and P. Y. Robin (1994), Modelling the evolution of columnar joints, *J. Volc. Geotherm. Res.*, *59*, 219–239.
- Burlini, L., S. Vinciguerra, G. Di Toro, G. De Natale, P. Meredith, and J. P. Burg (2007), Seismicity preceding volcanic eruptions: New experimental insights, *Geology*, *35*, 183–186, doi:10.1130/G23195A.1.
- Burlini, L., G. Di Toro, and P. Meredith (2009), Seismic tremor in subduction zones: Rock physics evidence, *Geophys. Res. Lett.*, *36*, L08305, doi:10.1029/2009GL037735.
- Cabrera, A., R. F. Weinberg, H. Wright, S. Zlotnik, and R. Cas (2011), Melt fracturing and healing: A mechanism for degassing and origin of silicic obsidian, *Geology*, *39*, 67–70.
- Cox, S. J. D., and P. G. Meredith (1993), Microcrack formation and material softening in rock measured by monitoring acoustic emissions, *Int. J. Rock Mech. Min. Sci. Geomech. Abstr.*, *30*, 11–24.
- David, C., B. Menendez, and M. Darot (1999), Influence of stress-induced and thermal cracking on physical properties and microstructure of La Peyratte granite, *Int. J. Rock Mech. Min. Sci.*, *36*, 433–448.
- Evans, A. G. (1974), The role of inclusions in the fracture of ceramic materials, *Asian J. Mater. Sci.*, *9*(7), 1145–1152.
- Evans, A. G. (1978), Microstructure from thermal expansion anisotropy—I. Single phase systems, *Acta Meta.*, *26*, 1845–1853.
- Fredrich, J. T., and T. Wong (1986), Micromechanics of thermally induced cracking in three crustal rocks, *J. Geophys. Res.*, *91*, 12,743–12,764, doi:10.1029/JB091iB12p12743.
- Gaunt, H. E., P. R. Sammonds, P. G. Meredith, and A. Chadderton (2016), Effect of temperature on the permeability of lava dome rocks from the 2004–2008 eruption of Mount St. Helens, *Bull. Volcanol.*, doi:10.1007/s00445-016-1024-5.
- Gudmundsson, A. (2006), How local stresses control magma-chamber ruptures, dyke injections, and eruptions in composite volcanoes, *Earth Sci. Rev.*, *79*, 1–31.
- Gudmundsson, A. (2011), *Rock Fractures in Geologic Processes*, Cambridge Univ. Press, Cambridge.
- Gudmundsson, A. (2012), Strengths and strain energies of volcanic edifices: Implications for eruptions, collapse calderas, and landslides, *Nat. Haz. Earth Sys. Sci.*, *12*(7), 2241–2258.
- Hatton, C. G., I. G. Main, and P. G. Meredith (1994), Non-universal scaling of fracture length and opening displacement, *Nature*, *367*, 160–162.
- Heap, M. J., Y. Lavallée, A. Laumann, K. U. Hess, P. G. Meredith, D. B. Dingwell, S. Huismann, and F. Weise (2013a), The influence of thermal-stressing (up to 1000°C) on the physical, mechanical, and chemical properties of siliceous-aggregate, high-strength concrete, *Constr. Build. Mater.*, *42*, 248–265.
- Heap, M. J., S. Mollo, S. Vinciguerra, Y. Lavallée, K.-U. Hess, D. B. Dingwell, P. Baud, and G. Iezzi (2013b), Thermal weakening of the carbonate basement under Mt. Etna volcano (Italy): Implications for volcano instability, *J. Volc. Geotherm. Res.*, *250*, 42–60.
- Johnson, B., A. F. Gangi, and J. Handin (1978), Thermal cracking of rock subjected to slow, uniform temperature changes, in *19th US Symposium on Rock Mechanics (USRMS)*, American Rock Mechanics Association.
- Jones, C., G. Keaney, P. G. Meredith, and S. A. F. Murrell (1997), Acoustic emission and fluid permeability measurements on thermally cracked rocks, *Phys. Chem. Earth*, *22*, 13–17.
- Julian, B. R., G. R. Foulger, F. C. Monastero, and S. Bjornstad (2010), Imaging hydraulic fractures in a geothermal reservoir, *Geophys. Res. Lett.*, *37*, L07305, doi:10.1029/2009GL040933.
- Kitao, K., K. Aiki, H. Watanabe, and K. Wakita (1990), Cold-water well stimulation experiments in the Sumikawa Geothermal field, Japan, *Geotherm. Resour. Counc. Trans.*, *14*, 1219–1224.
- Main, I. (1992), Earthquake scaling, *Nature*, *357*, 27–28.
- McNutt, S. R. (2000), Volcanic seismology, in *Encyclopedia of Volcanoes*, edited by H. Sigmundsson *et al.*, pp. 1015–1033, Academic Press, San Diego, California.
- Meredith, P. G., K. S. Knight, S. A. Boon, and I. G. Wood (2001), The microscopic origin of thermal cracking in rocks: An investigation by simultaneous time-of-flight neutron diffraction and acoustic emission monitoring, *Geophys. Res. Lett.*, *28*, 2105–2108, doi:10.1029/2000GL012470.
- Miller, A. D., B. R. Julian, and G. R. Foulger (1998), Three-dimensional seismic structure and moment tensors of non-double-couple earthquakes at the Hengill-Grensdalur volcanic complex, Iceland, *Geophys. J. Int.*, *133*, 309–325.

- Mollo, S., M. J. Heap, D. B. Dingwell, K. U. Hess, G. Iezzi, M. Masotta, P. Scarlato, and S. Vinciguerra (2013), Decarbonation and thermal micro-cracking under magmatic P-T-fco₂ conditions: The role of skarn substrata in promoting volcanic instability, *Geophys. J. Int.*, *195*, 369–380.
- Pyle, D. M., and J. R. Elliott (2006), Quantitative morphology, recent evolution, and future activity of the Kameni Islands volcano, Santorini, Greece, *Geosphere*, *2*, 253–268.
- Richter, D., and G. Simmons (1974), Thermal expansion behaviour of Igneous Rocks, *Int. J. Rock Mech. Min. Sci. Geomech. Abstr.*, *15*, 145–148.
- Simmons, G., and H. W. Cooper (1978), Thermal cycling cracking in three igneous rocks, *Int. J. Rock Mech. Min. Sci. Geomech. Abstr.*, *15*, 145–148.
- Tuffen, H., and D. B. Dingwell (2005), Fault textures in volcanic conduits: Evidence for seismic trigger mechanisms during silicic eruptions, *Bull. Volcanol.*, *67*, 370–387.
- Tuffen, H., D. B. Dingwell, and H. Pinkerton (2003), Repeated fracture and healing of silicic magma generate flow banding and earthquakes?, *Geology*, *31*, 1089–1092.
- Vinciguerra, S., C. Trovato, P. G. Meredith, and P. M. Benson (2005), Relating seismic velocities, thermal cracking and permeability in Mt. Etna and Iceland basalts, *Int. J. Rock Mech. Min. Sci.*, *42*, 900–910.
- Wang, H. F., and H. C. Heard (1985), Prediction of elastic moduli via crack density in pressurized and thermally stressed rock, *J. Geophys. Res.*, *90*(B12), 10,342–10,350.